Progress in Natural Science: Materials International 29 (2019) 440–446

HOSTED BY

Contents lists available at ScienceDirect

Progress in Natural Science: Materials International

journal homepage: www.elsevier.com/locate/pnsmi

Original Research

Influence of beam current on microstructure of electron beam melted Ti-6Al-4V alloy

Roman Laptev[a,*], Natalia Pushilina[a], Egor Kashkarov[a], Maxim Syrtanov[a], Ekaterina Stepanova[a], Andrey Koptyug[a,b], Andrey Lider[a]

[a] National Research Tomsk Polytechnic University, Tomsk, 634050, Russia
[b] Mid Sweden University, Östersund, SE-831 25, Sweden

ARTICLE INFO

Keywords:
Titanium alloy
Additive technology
Electron beam melting
Positron spectroscopy
Defects
Transmission electron microscopy

ABSTRACT

The defect microstructure of the samples manufactured from Ti-6Al-4V powder was studied using electron beam melting (EBM) in the beam current range of 17 - 13 mA. The hybrid digital complex combined positron lifetime spectroscopy and coincidence Doppler broadening spectroscopy was used to characterize the defect structure of the materials. The microstructure and defects were also analyzed by transmission electron microscopy. It has been established that the main type of the defects in the EBM manufactured samples is dislocations. According to the conducted measurements and calculations, the dislocation density in the EBM manufactured samples exceeds by two orders the similar value for the cast Ti-6Al-4Valloy. Formation of Ti-Ti-Al nanoscale clusters has been found in the EBM manufactured samples.

1. Introduction

Development of structural materials with high mechanical properties to be exploited in aggressive media is actual topic for the present-day materials science and engineering, aircraft engineering, aerospace industry, chemical and oil and gas industry. In recent years, the additive technologies represent promising and rapidly developing class of production of new materials with unique properties [1,2]. However, systemic studies of materials formation behavior are required for large-scale implementation of additive technologies into industry. The additive technologies open the opportunities to speed up the manufacturing process, enabling to save materials, produce lighter constructions with complex geometry that are impossible to obtain using conventional manufacturing techniques.

Electron beam melting (EBM) is one of the most demanded technologies to manufacture three dimensional metal products [3,4]. Unlike selective laser melting, electron beam melting technology does not require post processing, i.e., heat treatment to obtain high strength. EBM is typically used for dimension products manufacturing due to high productivity of the technology. However, the materials manufactured with additive technologies are characterized by specific types of macro- and microdefects conditioned by the specifics of physical processes taking place during additive technologies manufacturing [4–6]. The presence of such defects in the bulk of material can influence the mechanical properties (hardness, strength, lifetime, fracture toughness, etc.) of the products. Formation of defects in a material depends on many factors, such as electron beam current, scanning rate, powder particle size, hatching strategy and others [7–10]. In this respect, it becomes significant to optimize the manufacturing process of components produced by EBM, as well as to develop and implement non-destructive testing methods for quality control of additively manufactured products.

Positron spectroscopy techniques are used to control defects in manufactured products under additive technologies. These methods enable to investigate mechanisms and monitor dynamics of defect appearance, transformations and disappearance within the wide range of concentrations as well as defect dimensions. The positron annihilation lifetime spectroscopy (PALS) makes it possible to detect the defect types, monitor the dynamics in changes of defect concentration and size. Momentum distribution using coincidence Doppler broadening spectroscopy (CDBS) enables to get information about quality measurements of material structure, phase changes, chemical composition in locations of positron annihilation. Simultaneous application of these experimental techniques allows obtaining more detailed quality and quantity data on defect structure of the material. In this work, research of the defect structure of the EBM manufactured samples from Ti-6Al-

* Corresponding author.
E-mail addresses: laptevrs@tpu.ru (R. Laptev), pushilina@tpu.ru (N. Pushilina), egor_kashkarov@mail.ru (E. Kashkarov), maxim-syrtanov@mail.ru (M. Syrtanov), enstepanova@tpu.ru (E. Stepanova), andrey.koptyug@miun.se (A. Koptyug), lider@tpu.ru (A. Lider).

https://doi.org/10.1016/j.pnsc.2019.04.011
Received 15 October 2018; Received in revised form 29 April 2019; Accepted 30 April 2019
Available online 27 August 2019

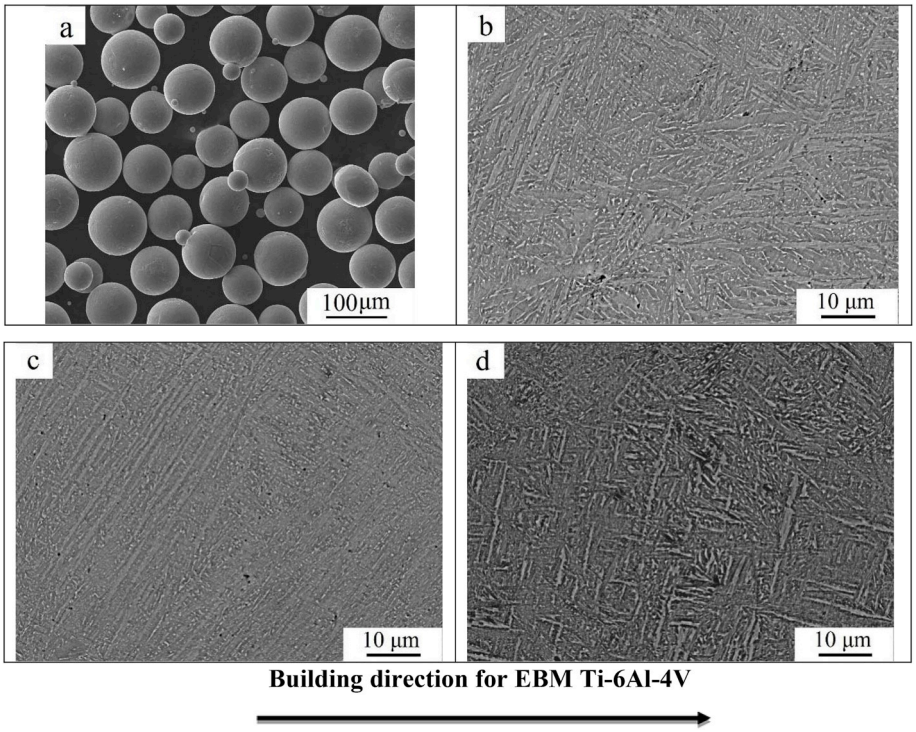

Fig. 1. Typical SEM images, (a) initial powder, EBM-built Ti-6Al-4V samples at I = (b) 17 mA, (c) 15 mA, (d) 13 mA.

4V powder depending on melting parameters has been performed using positron spectroscopy techniques, X-Ray structural analysis, and transmission electron microscopy.

2. Materials and methods

In this study the samples were prepared by EBM from spherical Ti-6Al-4V (Ti6Al4V ELI) powder using ARCAM A2 machine [11]. The samples were cylinders with the height of 2 mm and the diameter of 8 mm. The powder layer thickness was 70 μm. The samples were manufactured at the scanning rate of 3000 mm/s, electron beam power of 60 kW, and substrate temperature of ~700°C. Three series of the samples were prepared with the different values of the electron beam current during EBM: #1 – I = 17 mA, #2– I = 15 mA, #3 – I = 13 mA.

The structural and phase state of the obtained samples was examined using X-ray structural analysis, scanning electron microscopy (SEM), and transmission electron microscopy (TEM). The volume fractions and the lattice parameters of the phases were determined with the accuracy of ± 1% and 0.0001 nm, respectively, using Shimadzu XRD7000 diffractometer with Cu-K_α radiation source. Powder Cell program was used to identify the crystalline phases from diffraction patterns. The defect density and the presence of elastic stresses in titanium alloy were determined by the standard X-ray diffraction (XRD) methods, including the grazing angle technique, from the diffraction peak broadening at the half width using Cauchy approximation. The detailed microstructure analysis was carried out with SEM using S-4800 (Hitachi, Tokyo, Japan) and TEM using JEOL JEM-2100. The thin foil specimens for transmission electron microscopy were produced by jet electropolishing in the electrolyte mixture of 80 vol.% glacial acetic acid and 20 vol.% perchloric acid. The sizes of structural elements were measured from the relevant micrographs by the secant method.

The structure defects were analyzed with the positron spectroscopy techniques, and the hybrid digital complex with the system of external synchronization based on the modules of positron lifetime spectrometry and CDBS was used for positron lifetime spectroscopy. This hybrid digital complex was designed in Tomsk polytechnic university (TPU). The time resolution of the PALS module was 170 ± 7 ps, the count rate was 90 ± 30 counts/s. The count rate for the CDBS module was 116 ± 15 counts/s with the energy resolution of 1.16 ± 0.03 keV ^{44}Ti was used as the positron source with the activity of 0.91 MBq and positron maximum energy of 1.47 MeV. For each of the samples two PALS spectra and one two-dimensional CDBS spectrum statistically obtained $3{\cdot}10^6$ and $4{\cdot}10^7$, correspondingly.

Positron lifetime spectra processing was performed using the program software LT10 (ver. 10.2.2.2) [12,13] within the three-state positron trapping model [14]. Three time components τ_A, τ_B, τ_F with their intensity I_A, I_B, I_F, trapping rate k_A, k_B, and with average positron lifetime τ_{avg} were used for analysis. The spectra were analyzed in the series in which trapping rates k_A, k_B were combined for each pair of spectra of the same sample. At the same time components of positron lifetime τ_A, τ_B were combined for all spectra in the series. In this case, the value of lifetime of the positrons captured by A and B type defects as well as lifetime of delocalized positrons in Ti-6Al-4V lattice will be determined with high accuracy for all the spectra. The correction of the positron source input was performed with the empirical function determined earlier, the components of positrons annihilation in the source comprised τ_1 = 305 ± 1 ps (71.7%), τ_3 = 1779 ± 10 ps (28.3%), and the total source contribution was 5.9% for Ti-6Al-4V samples.

Two-dimensional CDBS spectra were analyzed with CDB Tools [15]. The conventional S and W parameters of CDBS were used for analysis [14]. The parameters were obtained for OX cross-section of two-dimensional spectrum [8]. The ratio curves R(E) = N(E)/N_0(E) were also analyzed for this cross-section where N(E) is the spectrum of the sample, and N_0(E) is the spectrum of the reference sample [16]. Defect-free technical pure titanium was used as the reference material N_0(E).

The microhardness of the samples was measured using Vickers hardness testing machine KB30S under the load of 0.5 kg. The average of 30 indentations was presented.

3. Results and discussion

Fig. 1 shows the SEM images of the initial powder (a) and EBM-built Ti-6Al-4V samples structure (b-d). The powder diameters are from 50 to 150 μm (Fig. 1a). Fig. 1b–d shows the detailed analysis of the EBM

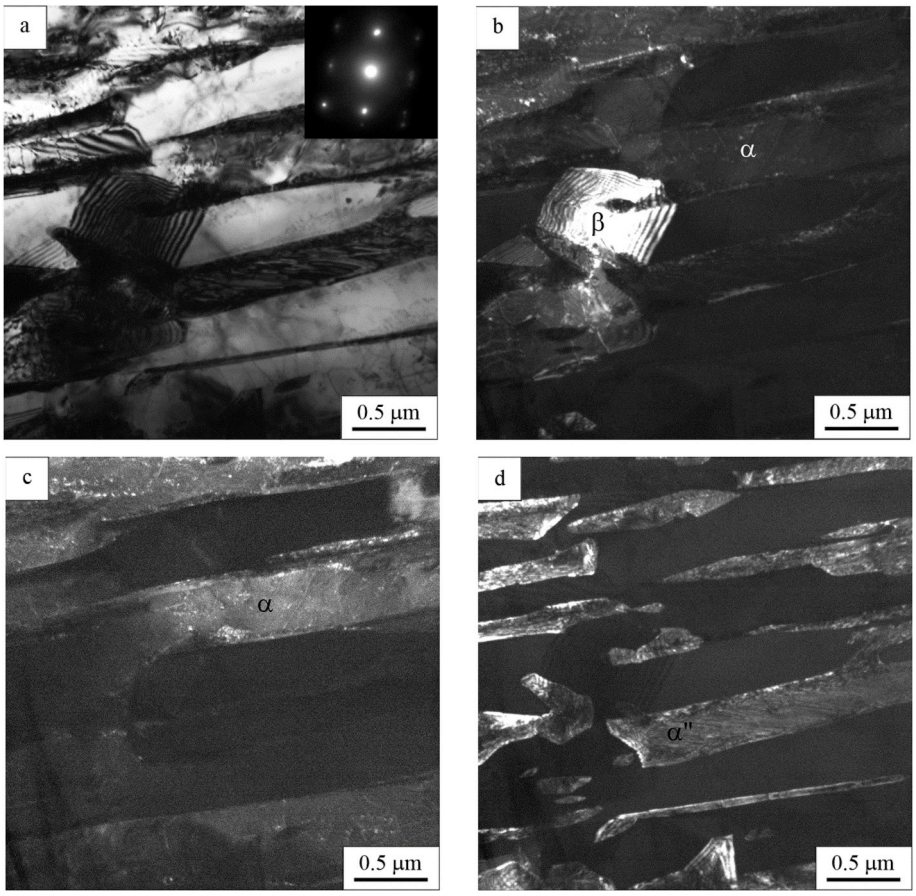

Fig. 2. Typical TEM images of the EBM Ti-6Al-4V alloy samples, (a) bright field image, (b–d) dark-field images (b - $(110)_{\beta\text{-Ti}}$ and $(101)_{\alpha\text{-Ti}}$ reflections, c – $(102)_{\alpha\text{-Ti}}$ reflection, d – $(111)_{\alpha''\text{-Ti}}$ reflection).

sample microstructure. This structure is Widmanstatten pattern with large variation in lath thickness. The bcc structure of β-phase in all samples is represented by discrete flat rods embedded in the continuous α-phase with hcp structure. The samples obtained with the use of different values of electron beam currents have different thickness of alpha plates. For example, thicker α lath is found in the samples prepared at the beam current 17 mA. In this case, in addition to the width of α laths in the structure which is mainly 0.4–0.6 μm, larger α plates with the width of 1.4–1.6 μm are also observed. The decrease in value of electron beam current from 17 to 13 mA leads to the reduction in the dimensions of α plates [6].

The detailed study of the microstructure of EBM Ti-6Al-4V samples using TEM revealed that the microstructure of all samples is similar when obtained at different beam current as demonstrated in Fig. 2. The dark-field images in Fig. 2b–c showed that the microstructure of the Ti-6Al-4V parts was represented by lamellar α phase with the transverse plate size varying mainly in the range of 0.2–0.6 μm in Fig. 2 c-d. At the same time, in addition to discrete flat rods embedded in the continuous α-phase detected by SEM, globular grains of 0.2–0.8 μm in size (Fig. 2a and b) are also present in the β phase. Formation of metastable martensitic α″ phase was also observed (Fig. 2d).

The XRD analysis indicated that all studied samples of EBM Ti-6Al-4V alloy were two-phase, containing the α-Ti (α′-Ti) phase with the hexagonal close-packed (hcp) lattice and β-Ti phase with the body-centered cubic (bcc) lattice [6]. The volume fraction of β phase in all investigated samples was about 3 vol. %. XRD studies also revealed that all samples of the Ti-6Al-4V alloy had different dislocation density $(1.7 \pm 0.1)\cdot 10^{13}\,m^{-2}$, $(1.6 \pm 0.1)\cdot 10^{13}\,m^{-2}$, and $(1.5 \pm 0.1)\cdot 10^{13}\,m^{-2}$ for samples #1, 2, and 3, respectively.

Fig. 3 presents the spectra of time distribution of positron annihilation in EBM Ti-6Al-4V samples at the variation of the current beam.

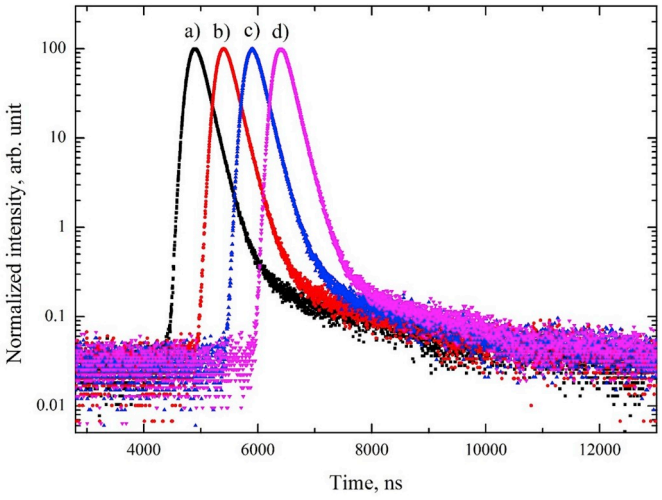

Fig. 3. The spectra of momentum distribution of positron annihilation in cast Ti-6Al-4V (a) and EBM manufactured Ti-6Al-4V samples at the currents of 17 mA (b), 15 mA (c), and 13 mA (d).

Table 1 represents the results of analysis for the experimental samples spectra with LT10 program under the three-state positron trapping model. In addition, all the parameters were compared to that of the positron annihilation in Ti-6Al-4V alloy manufactured using traditional techniques (casting) and then annealed at the temperature of 750°C for 24 h. It has been established that the only component

Table 1
Parameters of positron annihilation in the experimental samples.

State	τ_A, ps	I_A, %	τ_B, ps	I_B, %	k_A, ns^{-1}	k_B, ns^{-1}	τ_F, ps	I_F, %	τ_{avg}, ps
Cast	–	–	–	–	–	–	147 ± 1	100	147 ± 1
#1	164 ± 2	13	290 ± 5	0.06	0.11 ± 0.3	0.002 ± 0.001	147 ± 1	87	149 ± 1
#2	165 ± 2	20	291 ± 5	< 0.01	0.17 ± 0.3	< 0.001	148 ± 1	90	149 ± 1
#3	166 ± 2	15	287 ± 5	< 0.01	0.13 ± 0.3	< 0.001	148 ± 1	85	149 ± 1

$\tau_F = 147 \pm 1$ ps (Table 1) is present in the annealed Ti-6Al-4V alloy. According to the literature data, this component is related to the positron annihilation from delocalized state in titanium lattice [17–21]. As two other time reasoning components are absent in the spectra, it can be concluded that dislocation density and vacancy concentration are below the method detection limit (for vacancies $< 10^{-6}$ at. %, dislocation density $< 10^{12} cm^{-2}$), therefore the sample can be conditionally considered as zero-defects one [22].

In all the EBM manufactured samples in addition to the component $\tau_F = 147$ ps, there are two components distinguished which are responsible for annihilation of positrons captured by defects: $\tau_A = 165 \pm 2$ ps and $\tau_B = 291 \pm 5$ ps The component $\tau_A = 165 \pm 2$ ps is related to annihilation of positrons trapped in dislocations [23,24]. The long-lived component $\tau_B = 291 \pm 5$ ps is responsible for annihilation of positrons trapped in vacancies. In the latter case, positron lifetime in 1.8–4.1 times exceeds the lifetime of positrons in delocalized state depending on a number of vacancies [24–28]. Comparing the obtained value τ_B with the literature data it can be concluded that this component corresponds to vacancy complexes comprised of N = 4 vacancies (tetravacancies – 4 V) [27–29].

Based on the three-state positron trapping model, the concentration of dislocations C_d and tetravacancies C_{4V} in the samples can be determined with the following formulas [30]:

$$C_d = \frac{k_A}{\mu_d};$$

$$C_{4V} = \frac{k_B}{\mu_{4V}},$$

where, k_A, k_B – positron trapping rate in dislocations and tetravacancies, correspondingly, and μ_d, μ_{4V} – the positron trapping efficiency in dislocations and tetravacancies, respectively. The positron trapping efficiency is within the range of $(10^{-5} \div 10^{-4})$ $m^{-2} \cdot s^{-1}$ for most of the metals, the efficiency is $\mu_d = 0.5 \cdot 10^{-5} m^2 s^{-1}$ for titanium and its alloys [23–25]. The positron trapping efficiency in monovacancies μ_{1V} comprises $2 \cdot 10^{14}$ s^{-1} for metals, while for small vacancy concentrations ($m < 10$) the trapping efficiency μ_{mV} is in direct proportion to the number of vacancies N in this cluster. Thus, the positron trapping efficiency for tetravacancies will be $\mu_{4V} = 8 \cdot 10^{14}$ s^{-1} [29,31].

The calculated results of defect concentrations in EBM Ti-6Al-4V samples are represented in Table 2. It has been established that dislocation density in the EBM manufactured samples is more than in two orders greater than of cast material. The decrease in the beam current from 17 to 15 mA leads to slight increase within the margin of uncertainty in dislocation density and decrease in tetravacancies concentration. With further decrease of the beam current from 15 to 13 mA, dislocation density in the samples is comparable to the values C_d of the samples in the series #1.

Table 2
Defect concentration in the EBM manufactured Ti-6Al-4V samples.

State	Dislocations density C_d, $\times 10^{13} m^{-2}$	Tetravacancies concentration, ppm
Cast	< 0.01	< 0.001
#1	2.2 ± 0.9	0.003 ± 0.002
#2	3.3 ± 1.5	< 0.001
#3	2.4 ± 1.0	< 0.001

Taking into account the uncertainty for dislocation density obtained by the PALS and XRD methods, it can be concluded that the data is in good agreement.

Formation of nanoscale clusters and intermetallic Ti_3Al proto-precipitates under various effects is characteristic for titanium alloys including Ti-6Al-4V [32–35]. However, the positron lifetime spectrometry technique does not allow differentiating the annihilation contribution in titanium matrix and in Ti_3Al as positron lifetime is practically identical in these states [36]. Formation of nanoscale clusters Ti_3Al can be registered with CDBS. Fig. 4 presents two-dimensional spectra of CDBS. Based on the analysis of the median cross-section on X axis, it is possible to determine the S and W parameters that allow evaluating the defect level of materials. The values of the S and W parameters are presented in Table 3.

The increase in defects concentrations (vacancies and tetravacancies) leads to the S parameter increase and the W parameter decrease, which serves as the evidence of free volume formation. Therefore, the data from CDBS completely confirms the conclusions obtained after the analysis of the positron lifetime spectra.

To study the chemical environment effects inside the annihilation locations, two-dimensional spectra of the CDBS were obtained for titanium, aluminum, and vanadium after high temperature vacuum annealing. Fig. 5 presents the ratio curves of momentum distribution of positron annihilation for all the spectra where defect-free commercially pure titanium was used as the reference sample. In addition, Fig. 5b shows the graph of S = f(W). According to Ref. [37], if the experimental values of the parameters S and W for the set of samples are in the straight line of the plot S = f(W), this means that the predominant positron traps in the samples are the similar type of defect.

Fig. 5a shows that the ratio curves of momentum distribution of positron annihilation for commercially pure titanium and cast Ti-6Al-4V alloy have practically coincided. In the higher energy region (the core electron region), a slight line shift to aluminum line was observed for all the EBM manufactured Ti-6Al-4V samples. This shift serves as the evidence that during EBM the nanoscale clusters (Ti-Ti-Al) are being formed that leads to formation of proto-precipitates in the Ti_3Al phase [38,39]. Since the values for the all EBM Ti-6Al-4V samples are on the same straight line with the cold-rolled samples (Fig. 5b), it can be concluded that for all samples the prevailing type of defects are dislocations, which agrees well with PALS data.

To study the mechanical properties of the EBM manufactured samples, the Vickers microhardness was measured under the maximum indentation load of 0.5 kg (Fig. 6). It has been seen that the microhardness of EBM samples was significantly higher (in 20 HV and greater) than microhardness of the cast Ti-6Al-4V alloy. The linear tendency of the decrease of the average microhardness with the increase of the beam current during EBM has been observed. Usually, the hardness of a sample is determined by the phase composition, microstructure and defect structure of an alloy. On the one hand, formation of finer lamellar microstructure in the EBM manufactured samples leads to hardness increase when compared to cast alloy. This phenomenon is also observed in other research works [6]. On the other hand, high values of microhardness could be caused by high dislocation density in the EBM manufactured samples of Ti-6Al-4V alloy.

Therefore, the formation of the microstructure and phase state of the samples takes place as the result of melting up to the temperature of

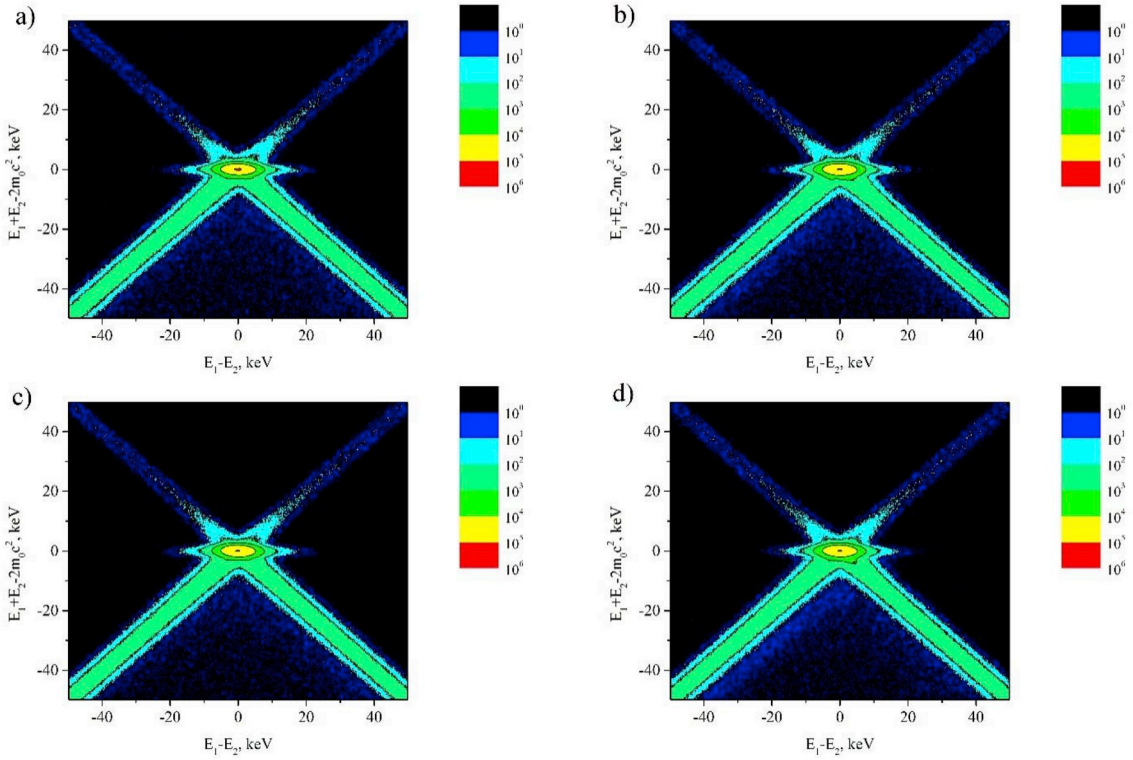

Fig. 4. Two dimensional spectra of Doppler broadening of the annihilation line: (a)–cast material; (b)–#1; (c)–#2; (d)–#3, listed in Table 1.

Table 3
Analysis of two-dimensional spectra of CDBS in the EBM manufactured Ti-6Al-4V samples.

State	S ± 2·10^{-4}	W ± 5·10^{-5}
Cast	0.5258	0.03324
#1	0.5287	0.03264
#2	0.5293	0.03242
#3	0.5278	0.03273

1900°C, subsequent rapid cooling to the temperature of ~720°C and followed by slow cooling up to the room temperature [4]. In this case, the cooling rate of a material is determined by the width and depth of the molten region and correspondingly by its lifetime. High cooling rates during EBM can lead to grains fragmentation, dispersed release of the second-phase particles, stress increase in material and dislocation density increase. As we have established earlier [6], the decrease of the beam current from 17 to 13 mA leads to refinement of material components (sizes of α-plates, β phase interlayers). In Refs. [32,40], it has been established that the highest beam current leads to the largest size of the melting pool. Therefore, the decrease of the beam current from 17 to 13 mA leads to decrease in the size of α-plates due to smaller size of the melting pool and higher cooling rate.

4. Conclusion

Based on the analysis of the positron spectroscopy data, it has been established that the main type of defects in the EBM Ti-6Al-4V samples

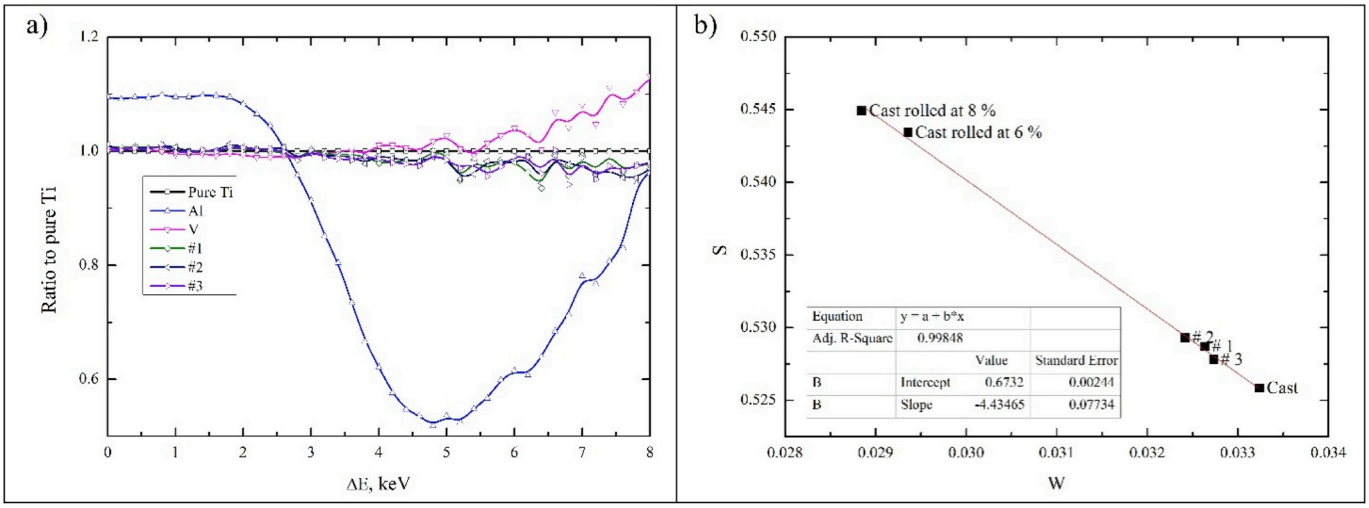

Fig. 5. (a) The ratio curves of momentum distribution of positron annihilation in the EBM manufactured Ti-6Al-4V samples; (b) S–W plot for the cold-rolled cast Ti-6Al-4V and the EBM manufactured Ti-6Al-4V samples.

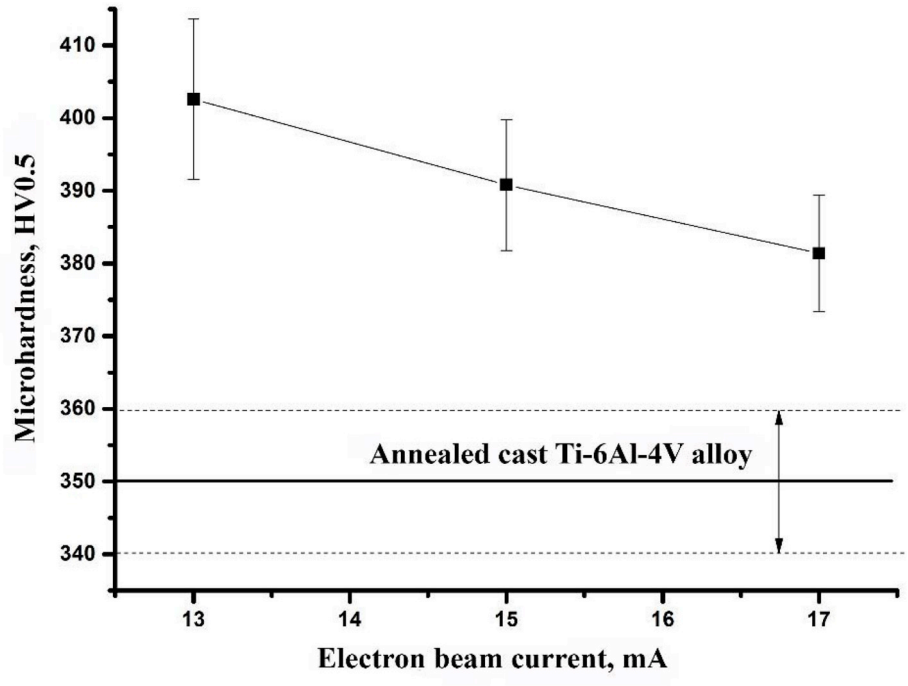

Fig. 6. Microhardness of the Ti-6Al-4V samples.

under study is dislocations. The characteristic of the samples manufactured with electron beam melting is the dislocation density that is by two orders greater than of the cast material after annealing. This difference is conditioned by the specifics of the temperature fields and stresses formed during the products manufacturing with metal powders melting. The microhardness of the EBM manufactured samples exceeds the microhardness of cast material. Decrease of the beam current allows obtaining the samples with higher microhardness.

Acknowledgement

The research was funded by Russian Science Foundation No17-79-20100. Lider A. and Koptyug A. acknowledge Tomsk Polytechnic University Competitiveness Enhancement Program for support with the development and preparation of the positron spectroscopy complex and samples.

References

[1] W.E. Frazier, J. Mater. Eng. Perform. 23 (2014) 1917–1928, https://doi.org/10.1007/s11665-014-0958-z.
[2] R.A. Katkar, R.M. Taft, G.T. Grant, Dent. Clin. N. Am. 62 (2018) 393–402, https://doi.org/10.1016/J.CDEN.2018.03.003.
[3] H. Attar, S. Ehtemam-Haghighi, D. Kent, M.S. Dargusch, Int. J. Mach. Tool Manuf. 133 (2018) 85–102, https://doi.org/10.1016/J.IJMACHTOOLS.2018.06.003.
[4] L.E. Murr, E. Martinez, K.N. Amato, S.M. Gaytan, J. Hernandez, D.A. Ramirez, et al., J. Mater. Res. Technol. 1 (2012) 42–54, https://doi.org/10.1016/S2238-7854(12)70009-1.
[5] N. Pushilina, A. Panin, M. Syrtanov, E. Kashkarov, V. Kudiiarov, O. Perevalova, et al., Metals (Basel) 8 (2018) 1–16, https://doi.org/10.3390/met8050301.
[6] N. Pushilina, M. Syrtanov, E. Kashkarov, T. Murashkina, V. Kudiiarov, R. Laptev, et al., Materials (Basel) 11 (2018) 763, https://doi.org/10.3390/ma11050763.
[7] A. Safdar, L.-Y. Wei, A. Snis, Z. Lai, Mater. Char. 65 (2012) 8–15, https://doi.org/10.1016/J.MATCHAR.2011.12.008.
[8] B. Vayssette, N. Saintier, C. Brugger, M. Elmay, E. Pessard, Procedia Eng. 213 (2018) 89–97, https://doi.org/10.1016/J.PROENG.2018.02.010.
[9] L.E. Murr, Addit. Manuf. 5 (2015) 40–53, https://doi.org/10.1016/J.ADDMA.2014.12.002.
[10] S.S. Al-Bermani, M.L. Blackmore, W. Zhang, I. Todd, Metall. Mater. Trans. A 41 (2010) 3422–3434, https://doi.org/10.1007/s11661-010-0397-x.
[11] American Society for Testing Materials, Standard Specification for Additive Manufacturing Titanium-6 Aluminum-4 Vanadium ELI (Extra Low Interstitial) with Powder Bed Fusion, (2014), https://doi.org/10.1520/F3001 West Conshohocken, P., USA.
[12] D. Giebel, J. Kansy, Mater. Sci. Forum 666 (2010) 138–141 https://doi.org/10.4028/www.scientific.net/MSF.666.138.
[13] D. Giebel, J. Kansy, Phys. Procedia 35 (2012) 122–127, https://doi.org/10.1016/j.phpro.2012.06.022.
[14] J. Čížek, J. Mater. Sci. Technol. 34 (2018) 577–598, https://doi.org/10.1016/J.JMST.2017.11.050.
[15] M. Petriska, V. Sabelová, V. Slugeň, Defect Diffus. Forum. 373 (2017) 71–74 https://doi.org/10.4028/www.scientific.net/DDF .373.71.
[16] J. Čížek, M. Vlček, I. Procházka, Nucl. Instrum. Methods Phys. Res. A. 623 (2010) 982–994, https://doi.org/10.1016/j.nima.2010.07.046.
[17] E. Stepanova, Y. Bordulev, V. Kudiiarov, R. Laptev, A. Lider, J. Xinming, AIP Conf. Proc. 1772 (2016) 030016, , https://doi.org/10.1063/1.4964554.
[18] R. Laptev, A. Lider, Y. Bordulev, V. Kudiiarov, G. Garanin, J. Alloys Compd. 645 (2015) S193–S195, https://doi.org/10.1016/j.jallcom.2014.12.257.
[19] R.S. Laptev, V.N. Kudiiarov, Y.S. Bordulev, A.A. Mikhaylov, A.M. Lider, Prog. Nat. Sci. Mater. Int. 27 (2017) 105–111, https://doi.org/10.1016/j.pnsc.2017.01.001.
[20] P. Hruška, J. Čížek, J. Knapp, O. Melikhova, L. Havela, S. Mašková, F. Lukáč, Acta Phys. Pol. A 132 (2017) 1606, https://doi.org/10.12693/APhysPolA.132.1606.
[21] P. Hruška, J. Čížek, F. Lukáč, J. Knapp, S. Mašková, J. Drahokoupil, et al., Defect Diffus. Forum. 373 (2017) 122–125 https://doi.org/10.4028/www.scientific.net/DDF.373.122.
[22] J. Čížek, I. Procházka, F. Bečvář, R. Kužel, M. Cieslar, G. Brauer, et al., Phys. Rev. B 69 (2004) 224106, https://doi.org/10.1103/PhysRevB.69.224106.
[23] N. Sultana, P.M.G. Nambissan, S. Datta, M.K. Banerjee, Phys. Procedia 35 (2012) 40–44, https://doi.org/10.1016/j.phpro.2012.06.008.
[24] N.M. Nancheva, K. Saarinen, G.S. Popov, Phys. Status Solidi A 95 (1986) 531–536, https://doi.org/10.1002/pssa.2210950221.
[25] Y. Shirai, M. Yamaguchi, Mater. Sci. Eng. A 152 (1992) 173–181, https://doi.org/10.1016/0921-5093(92)90064-8.
[26] M. Janeček, J. Stráský, J. Čížek, P. Harcuba, K. Václavová, V.V. Polyakova, et al., Metall. Mater. Trans. A 45 (2014) 7–15, https://doi.org/10.1007/s11661-013-1763-2.
[27] T.E.M. Staab, R. Krause-Rehberg, B. Kieback, R. Krause-Rehberg, B. Kieback, J. Mater. Sci. 34 (1999) 3833–3851, https://doi.org/10.1023/A:1004666003732.
[28] C.R. Luna, C. Macchi, A. Juan, A. Somoza, J. Phys. Conf. Ser. 443 (2013) 012019, , https://doi.org/10.1088/1742-6596/443/1/012019.
[29] J. Čížek, O. Melikhova, Z. Barnovská, I. Procházka, R.K. Islamgaliev, J. Phys. Conf. Ser. 443 (2013) 12008, https://doi.org/10.1088/1742-6596/443/1/012008.
[30] R. Krause-Rehberg, H.S. Leipner, Springer-Verlag Berlin and Heidelberg, Berlin, 1999.
[31] T.E.M. Staab, R. Krause-Rehberg, B. Vetter, B. Kieback, G. Lange, P. Klimanek, J. Phys. Condens. Matter 11 (1999) 1787–1806, https://doi.org/10.1088/0953-8984/11/7/010.
[32] M. Jamshidinia, F. Kong, R. Kovacevic, J. Manuf. Sci. Eng. 135 (2013) 061010, , https://doi.org/10.1115/1.4025746.
[33] F. Machado, J. Pabel, A. Luiggi, J. Comput. Methods Sci. Eng. 14 (2014) 53–71, https://doi.org/10.3233/JCM-130484.
[34] K. Yang, J. Huang, Y. Wang, Acta Mater. 51 (2003) 2577–2594, https://doi.org/10.1016/S1359-6454(03)00057-0.
[35] H. Carreon, D. San Martin, F. Caballero, V. Panin, Phys. Mesomech. 20 (2017)

447–456, https://doi.org/10.1134/S1029959917040105.
[36] Y. Shirai, T. Murakami, N. Ogawa, M. Yamaguchi, Intermetallics 4 (1996) 31–35, https://doi.org/10.1016/0966-9795(95)00014-P.
[37] L. Liszkay, C. Corbel, L. Baroux, P. Hautojärvi, M. Bayhan, A. Brinkman, S. Tatarenko, Appl. Phys. Lett. 64 (1994) 1380, https://doi.org/10.1063/1.111994.
[38] V.E. Panin, N.S. Surikova, A.M. Lider, Y.S. Bordulev, B.B. Ovechkin, R.R. Khayrullin, et al., Phys. Mesomech. 21 (2018) 452–463, https://doi.org/10.1134/S1029959918050090.
[39] H. Carreon, D. San Martin, F.G. Caballero, V.E. Panin, Phys. Mesomech. 20 (2017) 447–456, https://doi.org/10.1134/S1029959917040105.
[40] M. Jamshidinia, M.M. Atabaki, M. Zahiri, S. Kelly, A. Sadek, R. Kovacevic, J. Mater. Process. Technol. 226 (2015) 264–271, https://doi.org/10.1016/j.jmatprotec.2015.07.006.